Journal of
Materials Chemistry B

Materials for biology and medicine

rsc.li/materials-b

Indexed in Medline!

ROYAL SOCIETY OF CHEMISTRY
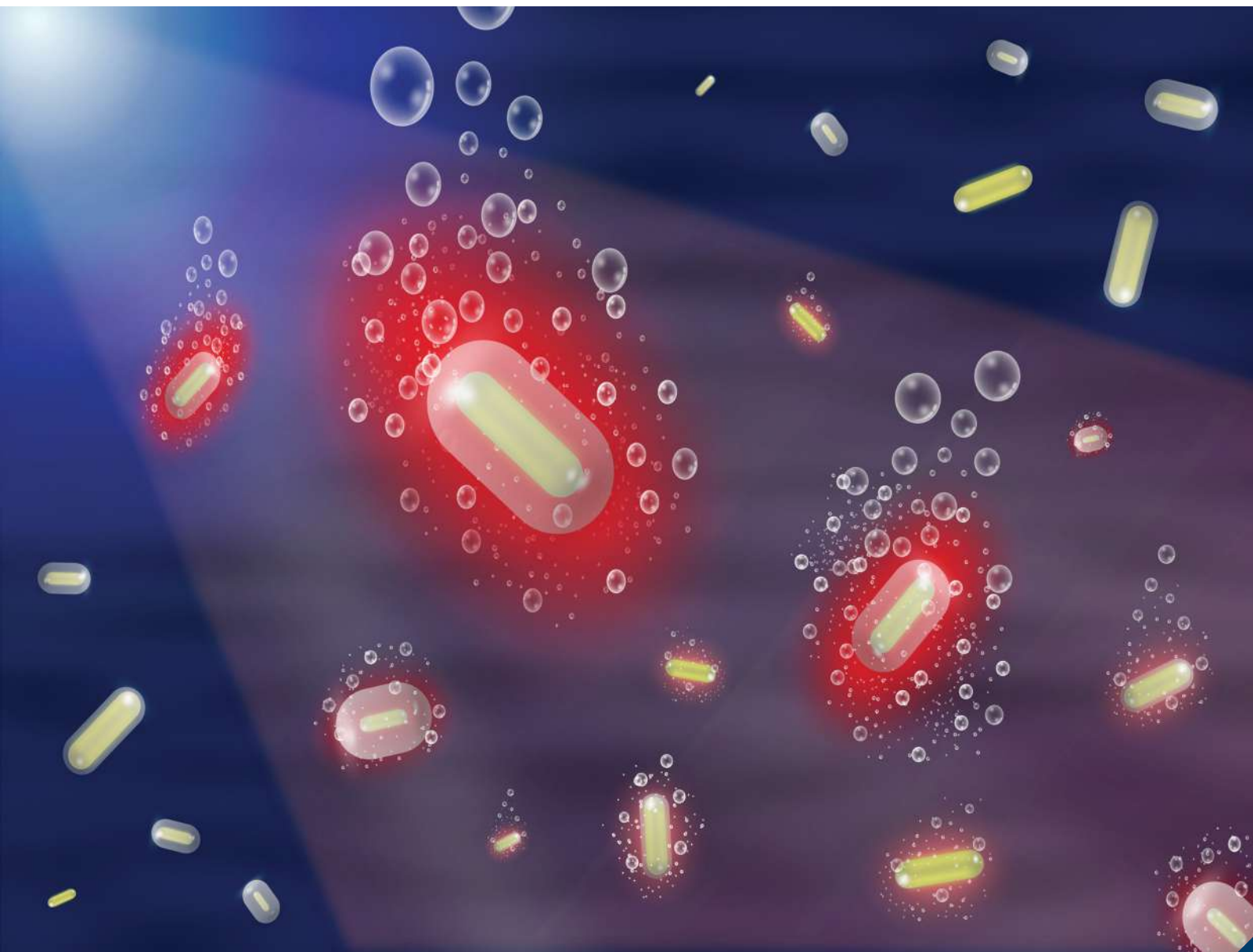
PAPER
Dong-Kwon Lim *et al.*
Precise control over the silica shell thickness and finding the optimal thickness for the peak heat diffusion property of AuNR@SiO$_2$

PAPER

Check for updates

Precise control over the silica shell thickness and finding the optimal thickness for the peak heat diffusion property of AuNR@SiO₂†

Wonseok Yang, [ID] [a] Sandeep Kaur,[b] Yong Duk Kim,[a] Jung-Mu Kim,[c] Seung Hee Lee[b] and Dong-Kwon Lim [ID] *[a]

Silica-coated gold nanorods (AuNRs) exhibit significantly enhanced photothermal effects and photoacoustic (PA) signal intensities, which is beneficial for various nanophotonic applications in materials science. However, the silica shell thickness for optimum enhancement is not fully understood and is even controversial depending on the physical state of the silica shell. This is because of the lack of systematic investigations of the nanoscale silica shell thickness and the photothermal effect. This study provides a robust synthetic method to control the silica shell thickness at the nanoscale and the physical state-dependent heat diffusion property. The selected base and solvent system enabled the production of silica-coated AuNRs (AuNR@SiO₂) with silica shell thicknesses of 5, 10, 15, 20, 25, 30, 35, and 40 nm. AuNRs with a 20 nm silica shell showed the highest photothermal effect with a 1.45-times higher photothermal efficiency than that of AuNRs without a silica shell. The low density of the silica shell on the AuNRs showed a low photothermal effect and photostability. It was found that the disruption of cetyltrimethyl ammonium bromide (CTAB) layers on the AuNRs was responsible for the low photostability of the AuNRs. The simulation study for the heat diffusion property showed facilitated heat diffusion in the presence of a 20 nm silica shell. In a cell-based study, AuNRs with a 20 nm silica shell showed the most sensitive photothermal effect for cell death. The results of this robust study can provide conclusive conditions for the optimal silica shell thickness to obtain the highest photothermal effect, which will be useful for the future design of nanomaterials in various fields of application.

1. Introduction

Gold nanorods (AuNRs) have been widely investigated because of their unique optical properties, such as strong and tunable light absorption in the near-infrared region according to the aspect ratio.[1–3] In particular, they absorb near infrared light more strongly than scattering it, so it is possible to apply AuNRs to various applications using the strong photothermal effect.[4–6] The photothermal effect can be widely utilized for noninvasive anticancer treatment, imaging applications such as photoacoustic (PA) imaging, and photonic polymerase chain reaction systems.[7–12] Nanomaterials possessing strong photothermal

effects and excellent photostabilities are essential for these applications. Interestingly, the photothermal effect and photostability of AuNRs could be further enhanced by forming a silica shell on the AuNRs. It is believed that the silica coating lowers the interfacial thermal resistance between the AuNR core and the surrounding solvent, allowing more heat to be released.[13] This is the origin of the enhanced photothermal effect and improved photostability of AuNRs during light illumination. The biological and colloidal stability of AuNRs can also be improved by the presence of a silica shell.[14–16] In this regard, the enhanced photo-physical properties of AuNRs can open new avenues for future bio-applications.[17,18]

However, the exact thickness and physical state of the silica shell for the highest enhancement of the photothermal effect are not clearly understood and controversial among the existing papers. For example, Chen *et al.* reported that the PA amplitude of AuNRs with a 20 nm silica shell was stronger than that of PEGylated AuNRs without a silica coating.[13] Furthermore, they reported that a silica shell thicker than 20 nm could contribute to lowering the local fluence of an incident laser by increasing light scattering, resulting in a decrease in the PA signal

[a] KU-KIST Graduate School of Converging Science and Technology, Korea University, 145 Anam-ro, Seongbuk-gu, Seoul 02841, Republic of Korea.
E-mail: dklim@korea.ac.kr

[b] Department of Nanoconvergence Engineering and Department of Polymer Nano-Science and Technology, Jeonbuk National University, Jeonju, Jeonbuk 54896, Republic of Korea

[c] Department of Electronic Engineering, Jeonbuk National University, Jeonju, Jeonbuk 54896, Republic of Korea

† Electronic supplementary information (ESI) available. See DOI: 10.1039/d1tb02288a

intensity as the temperature peak decreased and broadened. Nguyen *et al.* reported the highest heat transfer from AuNRs without a silica shell, in which time-resolved infrared spectroscopy was utilized to study the heat transfer efficiency around AuNRs. They reported that the slowest heat transfer rate was from AuNRs with a 30 nm mesoporous silica shell and the fastest was from AuNRs with a 90 nm mesoporous silica shell.[19] Pang *et al.* compared the PA signal intensity for Au nanospheres with diverse core sizes (5, 10, 15, and 20 nm) and silica shell thicknesses of 0, 10, 20, 30, and 40 nm, respectively. The authors reported that the addition of a silica coating enhanced the heat transfer from the particles to the water and enhanced the PA signal amplitude from the silica-coated Au nanospheres, as compared to uncoated Au nanospheres. The magnitude of the signal attenuation increased as the shell thickness increased from 0 to 40 nm.[20]

Accordingly, a systematic study of the exact thickness and silica density for the highest enhancement of the photothermal effect is strongly required to understand the fundamental conditions and design for future applications. Additionally, the synthetic conditions for producing the nanoscale silica shell thickness on AuNRs have not been firmly established in spite of extensive reports of using the Stöber method for coating AuNRs.[21] This is also a key obstacle to performing a systematic investigation of the relationship between the exact thickness and silica density for the highest enhancement of the photothermal effect.

This study demonstrates a robust synthetic method to reproducibly obtain AuNRs with a nanoscale silica shell in the range of 5, 10, 15, 20, 25, 30, 35, and 40 nm. It was found that the selection of the base and solvent are significantly important in determining the thickness and morphology of the silica shell on the AuNRs. The thickness-dependent photothermal effect was accurately evaluated in distilled water (DW) and in cells with an 808 nm laser. Along with the study to unveil the colloidal instability of AuNRs by light, simulation studies of the electromagnetic (EM) field distribution and heat diffusion properties were performed to experimentally and theoretically understand the effect of the silica shell on the enhanced photothermal effect according to the silica shell thickness.

2. Experimental

2.1 Synthesis of CTAB–AuNRs

CTAB–AuNRs were synthesized by the seed-mediated growth method,[22] in which the seed solution was prepared by mixing 9.75 mL of CTAB (0.1 M) with 0.25 mL of HAuCl$_4$ (0.01 M) and 0.6 mL of a freshly prepared ice-cold NaBH$_4$ solution (0.01 M). The solution was stirred vigorously for 1–2 min and then maintained at 28 °C for 3 h. In the second step, a growth solution was prepared by adding 25 mL of HAuCl$_4$ (0.01 M), 4.0 mL of AgNO$_3$ (0.01 M), 4.0 mL of freshly prepared ascorbic acid (0.01 M), and 5.0 mL of HCl (1.0 M) to 450 mL of CTAB (0.1 M). A seed solution (5.0 mL) was added to this solution, and the reaction mixture was subjected to gentle shaking for

several seconds and was then kept undisturbed overnight at 28 °C. The solution color changed to purple with the formation of the AuNRs. The AuNR aspect ratio was estimated to be ~4.6, with an average length of 62.7 (±5.0) nm and width of 13.6 (±1.1) nm with a localized surface plasmon resonance peak (λ_{max}) at approximately 780 nm.

2.2 Synthesis of AuNR@SiO$_2$

To remove the excess CTAB, 30 mL of AuNR solution was centrifuged twice at 15 000 rcf and 10 000 rcf for 15 min. After discarding the supernatant, the AuNRs were re-dispersed in DW to set the absorbance value to ~1.0.[23] The as-prepared AuNR solution (9.0 mL; optical density (OD) at 780 nm: 1.0) was transferred to a 50 mL falcon tube. IPA (13.5 mL) was added and the solution was gently stirred, followed by the addition of 1.0 mL of 0.05 M NaOH. Finally, a variable amount (1150, 1175, 1200, 1225, 1250, 1275, 1300, and 1350 μL) of TEOS solution (0.05 M in IPA) was added under slow shaking. The solution mixture was gently shaken for 24 h. The solution was then centrifuged at 10 000 rcf for 15 min, the supernatant was discarded, and the particles were re-dispersed in DW.

2.3 Synthesis of low density silica-coated AuNRs (AuNR@LD-SiO$_2$)

To remove the excess CTAB, 10 mL of AuNR solution was centrifuged twice at 15 000 rcf and 10 000 rcf for 15 min. After discarding the supernatant, the AuNRs were re-dispersed in DW to set the absorbance value to ~1.0.[23] The as-prepared AuNR solution (9.0 mL; OD 1.0) was transferred to a 50 mL falcon tube. 90 μL of CTAB (0.5 M) was added and the solution was gently stirred, followed by the addition of 1.0 mL of 0.05 M NaOH. Finally, 50 μL of TEOS solution (1.0 M in IPA) was added under slow shaking. The solution mixture was gently shaken for 20 h. The solution was then centrifuged at 10 000 rcf for 15 min, the supernatant was discarded, and the particles were re-dispersed in DW.

2.4 Setup for photothermal effect

To investigate the photothermal effect of CTAB–AuNRs with and without silica shells, 2 mL of solution (OD at 780 nm: 0.5) in a quartz cell was irradiated with an 808 nm NIR laser at 1.25 W cm^{-2} for 5 min and then cooled naturally to room temperature for 10 min without laser irradiation. The temperature changes were monitored every 1 min.

2.5 Calculation of photothermal conversion efficiency

The temperature of a 2 mL sample solution was recorded every 1 min while irradiating the 808 nm CW laser for 5 min, and then naturally cooled to room temperature for 35 min. The photothermal conversion efficiency (η) was calculated using eqn (1).[24–26]

$$\eta = \frac{hS(T_{max} - T_{amb}) - Q_0}{I(1 - 10^{-A_{808}})} \quad (1)$$

where h and S are the heat transfer coefficient and surface area of the quartz cuvette covered by the sample, respectively; T_{max}

This journal is © The Royal Society of Chemistry 2022

J. Mater. Chem. B, 2022, **10**, 364–372 | **365**

and T_{amb} are the maximum temperatures under laser irradiation and the ambient temperature, respectively; Q_0 represents the heat dissipated due to solvent absorption under the 808 nm laser irradiation, which can be calculated by $Q_0 = 5.4 \times 10^{-4} \times I$ ($J\ s^{-1}$); and I and A_{808} are the incident laser power and absorbance of the solutions at 808 nm, respectively. To calculate hS, a dimensionless driving force temperature (θ) is introduced.

$$\theta = \frac{T - T_{amb}}{T_{max} - T_{amb}} \quad (2)$$

The sample system time constant, τ_s, can be calculated as follow (3).

$$t = -\tau_s \ln \theta \quad (3)$$

$$hS = \frac{m_s c_s}{\tau_s} \quad (4)$$

where m_s and c_s are the mass and heat capacity ($4.2\ J\ (g\ ^\circ C)^{-1}$) of the solution, and τ_s can be determined by applying the linear time data from the cooling time, t, *versus* the negative natural logarithm after the laser is switched off according to the equation.

2.6 Finite element method lab-based simulation studies

Two different types of finite element method (FEM) lab-based simulations, using Ansoft HFSSTM software (Ansys Inc., USA), for the EM field distribution and the heat transfer rate were performed to verify our experimental results using an orthogonal approach. The EM field of the AuNRs-3D-model in accordance with the thickness of the silica shell was calculated based on Maxwell's equations in HFSS. The relative permittivity and dielectric loss tangent of Au, SiO_2, and H_2O are (-24.718, -0.06277611), (2.1337, 0.001771149), and (1.7662, 2.15564-7), respectively, based on Johnson and Christy at a 808 nm wavelength.[27] The maximum enhanced EM field (E/E_{in}) can be calculated using the HFSS, and the Poynting vector can also be calculated using the calculated electric and magnetic field vectors. The heat transfer rate can be estimated through the Poynting vector, which represents the directional energy flux (the energy transfer per unit area per unit time) of an EM field.

2.7 Silica shell thickness-dependent photothermal effect in the cell

HSC-3 cells (10k) in 96 wells were incubated for 12 h with AuNRs dispersed in DMEM (100 µL), but with a controlled OD of the samples (that is, CTAB–AuNR (OD at 780 nm: 1.5), AuNR@SiO$_2$ (OD at 780 nm: 1.5) with a thickness of 5–15 nm, and AuNR@SiO$_2$ (OD at 780 nm: 2.0) with a thickness of 20–40 nm) to absorb the same amount of AuNRs in the cells. After replacing the cell culture media, each well was irradiated with an 808 nm CW laser for 90 s and washed with a colorless medium. The cell viability was determined using the 3-(4,5-dimethylthiazol-2-yl)-5-(3-carboxymethoxyphenyl)-2-(4-sulfophenyl)-2H-tetrazolium assay. The absorbance at 490 nm was measured using a plate reader.
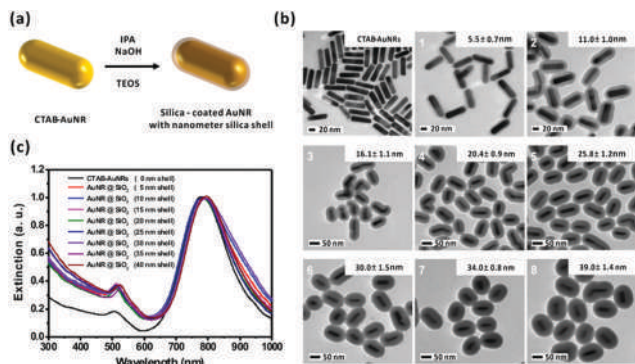
3. Results and discussion

3.1 Synthesis and characterization of AuNR@SiO$_2$

The formation of silica shells on AuNRs is often elusive because of the high failure rate in the synthesis.[28] For example, aggregation and the failure to obtain the desired thickness occurs frequently during the silica shell formation reaction.[17,29] Therefore, a robust synthetic method is required to produce silica shell-coated AuNRs with a nanoscale thickness. It was assumed that the conditions for hydrolysis with a base and the polycondensation of hydrolyzed silanol on AuNRs are critical in the typical Stöber method. The types of bases and solvents were focused on to examine their effect on the resulting silica shell thickness on the AuNRs. Two different bases, NaOH and NH$_4$OH, and three different solvents, methanol, ethanol, and isopropanol, were studied. First, CTAB-stabilized AuNRs (AR = 4.6:1, λ_{max} = 780 nm) were prepared by the seed-mediated growth method.[22] The excess amount of CTAB in the CTAB–AuNR solution was removed by double centrifugation. IPA (9.0 mL) was added to 6.0 mL of AuNRs (OD 1.0), and then 250 µL of different concentrations of NaOH (0.01, 0.05, 0.1 M) were added to the AuNR solution. Then, 1175 µL of 0.05 M TEOS (target thickness: 10 nm) was slowly dropped and shaken gently for 12 h. The use of NaOH as a hydrolysis agent at a low concentration (0.01 M) was not sufficient to produce a visible silica layer on the CTAB–AuNRs (Fig. S1(a), ESI†). Increasing the NaOH concentration to 0.05 M (resulting solution pH 11.9) led to uniform AuNRs@SiO$_2$ with a shell thickness of 10.2 ± 0.5 nm (Fig. S1(b), ESI†). Further increasing the NaOH concentration to 0.1 M, mainly resulted in a very thin silica layer of 1.6 ± 0.9 nm (Fig. S1(c), ESI†), because the AuNRs aggregated before being coated with silica due to the increased ionic strength which is favorable for AuNR aggregation at a high pH (12.7).[30] Additionally, as shown in Fig. S1(d) (ESI†), particle aggregation was visible in the UV spectrum when using 0.1 M NaOH, as compared to those using 0.01 M and 0.05 M NaOH.

A milder base, such as ammonia, was also investigated to evaluate the effect of varying amounts of NH$_4$OH (90, 180, and 270 µL) on the silica shell formation. The same TEOS amount (target thickness: 10 nm, 1175 µL of 0.05 M) was slowly dropped and gently shaken for 12 h. When 90 µL of NH$_4$OH (28%) was added to 6.0 mL of AuNRs (OD 1.0), the pH of the solution was found to be 11.8, which is identical to the pH of 0.05 M NaOH. However, the silica shell thickness on the CTAB–AuNRs was 4.1 ± 0.7 nm and the shell structure was not uniform (Fig. S1(e), ESI†). Increasing the amount of NH$_4$OH to 180 µL and 270 µL led to the thickness of the silica shell gradually increasing to 5.9 ± 1.5 nm and 12.0 ± 0.7 nm, respectively (Fig. S1(f and g), ESI†). However, the increased amount of NH$_4$OH resulted in particle aggregation in the UV spectrum (Fig. S1(h), ESI†).

Furthermore, the effect of solvent polarity on the shell formation reaction was investigated using three different alcoholic solvents (that is, MeOH, EtOH, and IPA). Using MeOH as a solvent did not produce a silica coating on the CTAB–AuNRs (Fig. S1(i), ESI†) because of the rapid hydrolysis of TEOS, which

366 | *J. Mater. Chem. B*, 2022, **10**, 364–372

This journal is © The Royal Society of Chemistry 2022

Fig. 1 (a) The synthetic scheme for AuNR@SiO$_2$ with a nanometer-scale silica shell; (b) TEM images and (c) UV-Visible spectra of CTAB–AuNRs and AuNR@SiO$_2$ with different silica shell thicknesses ((1) 5.5 ± 0.7, (2) 11.0 ± 1.0, (3) 16.1 ± 1.1, (4) 20.4 ± 0.9, (5) 25.8 ± 1.2, (6) 30.0 ± 1.5, (7) 34.0 ± 0.8, and (8) 39.0 ± 1.4 nm).

increases the nucleation rate and causes the formation of stable, very small silica nuclei in the solution, and not on the AuNRs.[31] When using EtOH, the hydrolysis of TEOS was expected to be slower than that of MeOH. However, the target thickness of the silica shell was not attained (4.3 ± 0.8 nm, Fig. S1(j), ESI†) in the EtOH solvent. In contrast, IPA enabled the successful formation of a silica shell on the AuNRs because of the relatively slow hydrolysis kinetics, which facilitated the silica shell formation on the AuNRs. A uniform silica shell at the target thickness was obtained on the AuNR surface (10.2 ± 0.5 nm, Fig. S1(k), ESI†) using IPA solvent.[31]

Next, the reaction conditions with a base (0.05 M NaOH) and a solvent (IPA) were examined to control the thickness of the silica shell at the nanoscale by varying the amount of TEOS (Fig. 1(a)). As shown in Fig. 1(b), the thickness of the silica shell on the CTAB–AuNRs increased linearly with an increase in the TEOS content. The thicknesses of the silica shells were 5.5 ± 0.7, 11.0 ± 1.0, 16.1 ± 1.1, 20.4 ± 0.9, 25.8 ± 1.2, 30.0 ± 1.5, 34.0 ± 0.8, and 39.0 ± 1.4 nm in the TEM analysis (Fig. 1(b)). The CTAB–AuNR spectral shape did not significantly change with the formation of the silica shell, but slight red-shifts (from 780 nm to 795 nm) of the peak plasmon band of AuNRs with a silica shell formation and thickness were observed (Fig. 1(c) and Fig. S2, ESI†). This shift is due to the increased local refractive index around the AuNRs generated by the silica shell, which has a higher refractive index (1.45) than water (1.33).[17,32,33]

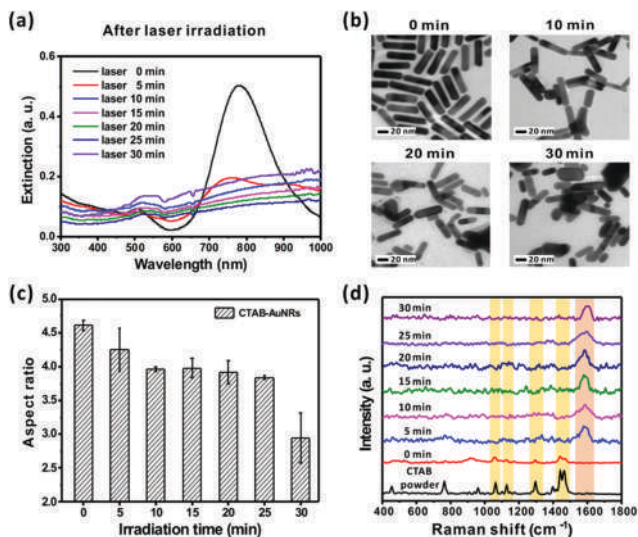### 3.2 Silica shell thickness-dependent photothermal properties and photostability of AuNR@SiO$_2$

The photothermal effect of AuNR@SiO$_2$ with a thickness of 5, 10, 15, 20, 25, 30, 35, and 40 nm was evaluated with a fixed OD (0.5 at 780 nm), volume (2.0 mL), and an 808 nm CW laser (Fig. S3, ESI†). The temperature was monitored every 1 min for 5 min, as shown in Fig. 2(a). No temperature increase was observed for DW. The CTAB–AuNRs showed an increase of up to 69.1 °C after 5 min of laser irradiation. After 5 min, the solution temperature of AuNR@SiO$_2$ with thicknesses of 5, 10,
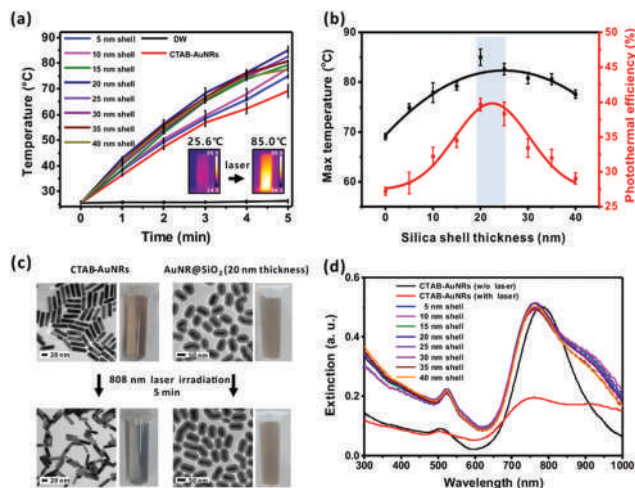
Fig. 2 (a) The temperature changes of DW, CTAB–AuNRs, and AuNR@-SiO$_2$ under irradiation of a 808 nm laser for 5 min; (b) the final temperatures and photothermal conversion efficiencies of CTAB–AuNRs and AuNR@SiO$_2$ with different silica shell thickness (5.5 ± 0.7, 11.0 ± 1.0, 16.1 ± 1.1, 20.4 ± 0.9, 25.8 ± 1.2, 30.0 ± 1.5, 34.0 ± 0.8, and 39.0 ± 1.4 nm); (c) TEM images and photographs of the CTAB–AuNR and AuNR@SiO$_2$ (20 nm) solution color before and after 5 min of laser irradiation; and (d) UV-Visible spectra after 5 min of laser irradiation.

15, 20, 25, 30, 35, and 40 nm showed rapid increases, and the final temperatures were 74.9, 77.9, 79.2, 85.0, 82.6, 80.8, 80.6, and 77.6 °C, respectively. AuNRs@SiO$_2$ with a thickness of 20 nm showed the highest photothermal effect, and the effect gradually decreased as the thickness increased beyond 20 nm (Fig. 2(b)). The photothermal conversion efficiency was calculated based on the results and parameters required, which were 27.21% for CTAB–AuNRs without a silica coating, 28.41% for AuNR@SiO$_2$ with 5 nm, 32.21% for AuNR@SiO$_2$ with 10 nm, 34.49% for AuNR@SiO$_2$ with 15 nm, 39.67% for AuNR@SiO$_2$ with 20 nm, 38.34% for AuNR@SiO$_2$ with 25 nm, 33.43% for AuNR@SiO$_2$ with 30 nm, 31.99% for AuNR@SiO$_2$ with 35 nm, and 29.05% for AuNR@SiO$_2$ with 40 nm (Fig. 2(b) and Fig. S4, ESI†). The photothermal conversion efficiency of AuNR@SiO$_2$ with a 20 nm thickness was 1.45 times higher than that of CTAB–AuNRs (Fig. 2(b)). These results are in good agreement with those reports that mentioned the enhanced photothermal effect with a silica thickness of 20 nm.[34,35] The decreased photothermal efficiency of AuNR@SiO$_2$ thicker than 20 nm is expected to be an increased contribution of the finite thermal conduction of silica and a decrease in local fluence due to an increased scattering.[13] Thereby, the thermal diffusion process is not efficient with increasing the silica shell thickness.

In addition to the photothermal effect, the photostabilities of CTAB–AuNRs and AuNR@SiO$_2$ were compared. After laser irradiation for 5 min, the color of the CTAB–AuNR solution changed to blue (Fig. 2(c)) and significant dampening of the spectral shape was observed, indicating the aggregation of AuNRs (Fig. 2(d)). The time-dependent UV-visible spectra showed complete dampening and morphological changes after 10 min (Fig. 3(a) and (b)). The aspect ratio of the CTAB–AuNRs decreased from approximately 4.6 ± 0.1 to 2.9 ± 0.4 (Fig. 3(c)).
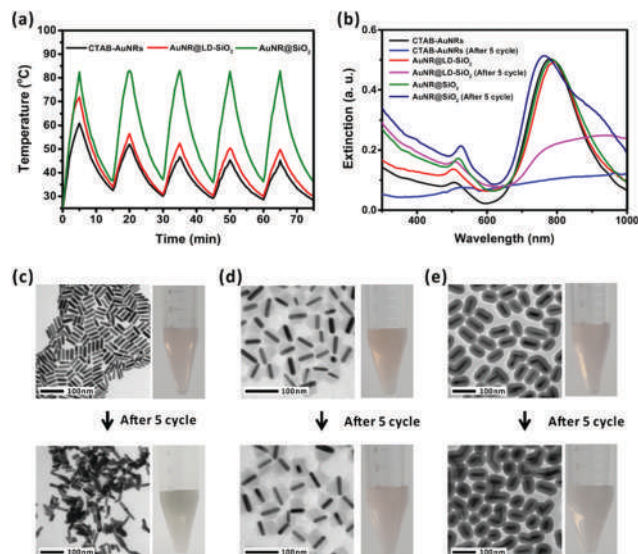
This journal is © The Royal Society of Chemistry 2022

J. Mater. Chem. B, 2022, **10**, 364–372 | **367**

Fig. 3 (a) The time-dependent change of the CTAB–AuNR UV-Visible spectra under an 808 nm laser irradiation; (b) TEM images of CTAB–AuNRs irradiated with an 808 nm laser (0, 10, 20, and 30 min); (c) the time-dependent change of the CTAB–AuNR aspect ratio under an 808 nm laser irradiation; and (d) Raman spectra changes of the CTAB–AuNRs under an 808 nm laser irradiation every 5 min.

Fig. 4 (a) The temperature changes of CTAB-AuNRs (OD 0.5, 2 mL), AuNR@LD-SiO$_2$ (OD 0.5, 2 mL), and AuNR@SiO$_2$ (OD 0.5, 2 mL) with the light on (5 min) and off (10 min); (b) UV-Visible spectra and TEM images and photographs of the (c) CTAB-AuNR, (d) AuNR@LD-SiO$_2$, and (e) AuNR@SiO$_2$ solution color before and after light illumination (5 cycles).

Raman analysis showed that the CTAB stabilizer on the AuNRs had been removed under light illumination (Fig. 3(d)), which is the primary reason for the low colloidal stability of the AuNRs. The CTAB on the AuNRs before laser irradiation showed Raman peaks at 1062, 1127, 1295, 1441, and 1464 cm^{-1}, which can be attributed to the vibration modes of –C–C–, –CH$_2$–, and –CH$_3$– in CTAB (Fig. S5, ESI†).[36] However, after 5 min of laser irradiation, the Raman peaks at 1062, 1127, 1295, 1441, and 1464 cm^{-1} disappeared and a new peak appeared at 1600 cm^{-1}, which is a typical carbonaceous peak (Fig. 3(d)).[37]

In contrast, AuNR@SiO$_2$ showed no significant changes in the nanostructures.[38,39] As shown in Fig. 2(d), a blue shift (20–30 nm) and a broadened spectral shape at 900 nm were observed, but the intensity of AuNR@SiO$_2$ did not decrease. Although the broadening of the spectral shape at 900 nm was not significant, the dampening of the broad new peak at 950 nm was greater in the case of AuNR@SiO$_2$ with 35 nm and 40 nm, indicating that a thicker silica shell is not desirable for fast heat diffusion. The results conclusively indicate that the presence of a 20–25 nm silica shell is desirable to attain the highest photothermal effect and enhanced photostability.[14]

3.3 The effect of density and morphology of the silica shell on the AuNRs

Along with thickness, the physical states (that is, density and morphology) of the silica shell on the AuNRs are expected to be a significant factor in the photothermal performance and photostability.[40] The AuNRs with two different physical states of the silica shell (that is, low density with non-uniform shell structures and dense with a uniform shell, but with a 20 nm thickness) were compared in terms of photothermal efficiency and photostability. A low density, non-uniform silica shell on the AuNRs (AuNR@LD-SiO$_2$) with a thickness of 20 nm was prepared (Section 2.5). As shown in Fig. S6 (ESI†), the density of the silica shell on the AuNRs could be identified from the TEM images, XRD, and XPS analysis. The TEM image of AuNR@LD-SiO$_2$ showed a weak contrast and non-uniform shell structure, which is clearly distinguishable from that of AuNR@SiO$_2$. The characteristic peaks of SiO$_2$ could be identified at $2\theta = 20$–$24°$ in the XRD analysis.[41] Because of the low density of SiO$_2$ in the AuNR@LD-SiO$_2$, a much weaker peak intensity of SiO$_2$ than that of AuNR@SiO$_2$ was observed. The (111), (200), (220), (311), and (222) diffraction peaks are the characteristic peaks of the Au cubic phase. XPS analysis showed the low amount of Si in case of AuNR@LD-SiO$_2$ compared with that of AuNR@SiO$_2$.[42]

The photothermal efficiency and photostability of CTAB–AuNRs, AuNR@SiO$_2$, and AuNR@LD-SiO$_2$ were investigated by repeating five cycles with light illumination for 5 min and natural cooling for 10 min at a fixed OD (0.5 at 780 nm) and volume (2.0 mL). As shown in Fig. 4(a), AuNR@LD-SiO$_2$ with 20 nm showed a higher photothermal effect than the CTAB–AuNRs and a slightly lower photothermal effect than the AuNR@SiO$_2$ in the first cycle. However, the peak temperature (71.8 °C) of AuNR@LD-SiO$_2$ observed in the first cycle showed a sharp decrease (56.5 °C) in the second cycle, which was approximately 68% of AuNR@SiO$_2$, and then decreased gradually with increasing cycles. In contrast, AuNR@SiO$_2$ showed highly uniform peak temperatures. The final temperatures in each cycle were 82.5, 83.0, 83.0, 82.7, and 82.9 °C, respectively, showing a highly narrow standard deviation (±0.19 °C). The photothermal efficiency did not change significantly. The temperature increase rates in each cycle were 11.5, 9.9, 9.6, 9.4, and 9.5 °C min^{-1}, respectively. Table 1 summarizes both parameters (final temperature and temperature increase rate) of the CTAB–AuNR and AuNR@LD-SiO$_2$.

368 | J. Mater. Chem. B, 2022, 10, 364–372

This journal is © The Royal Society of Chemistry 2022

Table 1 The final temperature and temperature increase rate in each thermal cycle of AuNR@SiO$_2$, AuNR@LD-SiO$_2$, and CTAB–AuNRs

|		Cycle 1	Cycle 2	Cycle 3	Cycle 4	Cycle 5	Mean (±STDV)
AuNR@SiO$_2$	Final temp. (°C)	82.5	83.0	83.0	82.7	82.9	82.8 (±0.19)
	Increase rate (°C min^{-1})	11.5	9.9	9.6	9.4	9.5	10.0 (±0.77)
AuNR@LD-SiO$_2$	Final temp. (°C)	71.8	56.5	52.4	50.4	49.8	56.2 (±8.15)
	Increase rate (°C min^{-1})	9.8	4.6	4.5	4.1	4.1	5.4 (±2.20)
CTAB–AuNRs	Final temp. (°C)	60.9	52.0	46.7	45.3	45.2	50.0 (±5.98)
	Increase rate (°C min^{-1})	7.4	4.1	3.4	3.3	3.2	4.3 (±1.58)

A sharp decrease in the photothermal efficiency of AuNR@LD-SiO$_2$ was expected from the low photostability of AuNR@LD-SiO$_2$. As shown in Fig. 4(b), the UV-visible spectra of AuNR@LD-SiO$_2$ exhibited a red shift and significant dampening. However, the UV-visible spectra of AuNR@SiO$_2$ showed a blue shift (20–30 nm) and slight spectral broadening after five cycles. TEM images and photographs of the solution before and after five cycles showed a change in the AuNR structure of CTAB–AuNR and AuNR@LD-SiO$_2$ (Fig. 4(c)–(e)). These results indicate that dense and uniform silica shells on AuNRs is a critical factor for enhancing the photothermal effect and improving photostability.

3.4 FDTD simulation studies

FDTD simulation studies were conducted to theoretically understand why the 20 nm silica shell enhanced the photothermal efficiency.[19,23] First, the EM field distributions when the light was incident on AuNR and AuNR@SiO$_2$ was calculated, and then the heat diffusion property with an increasing silica shell thickness was calculated. Fig. 5(a) shows that the EM fields were strongly distributed around both ends of the AuNRs when the incident excitation wavelength was 808 nm. The peak values of the enhanced EM fields (E/E_{in}) of the AuNRs were calculated by increasing the thickness of the silica shell. The peak EM fields (E/E_{in}) increased according to the thickness of the silica shell until the thickness reached 20 nm. Unlike the experimental results, the peak EM field did not decrease even when the silica shell thickness exceeded 20 nm (Fig. 5(b)). Because the silica shell is optically transparent in the 808 nm range,[43] an enhanced EM field can be expected from the further localization of the initial field on
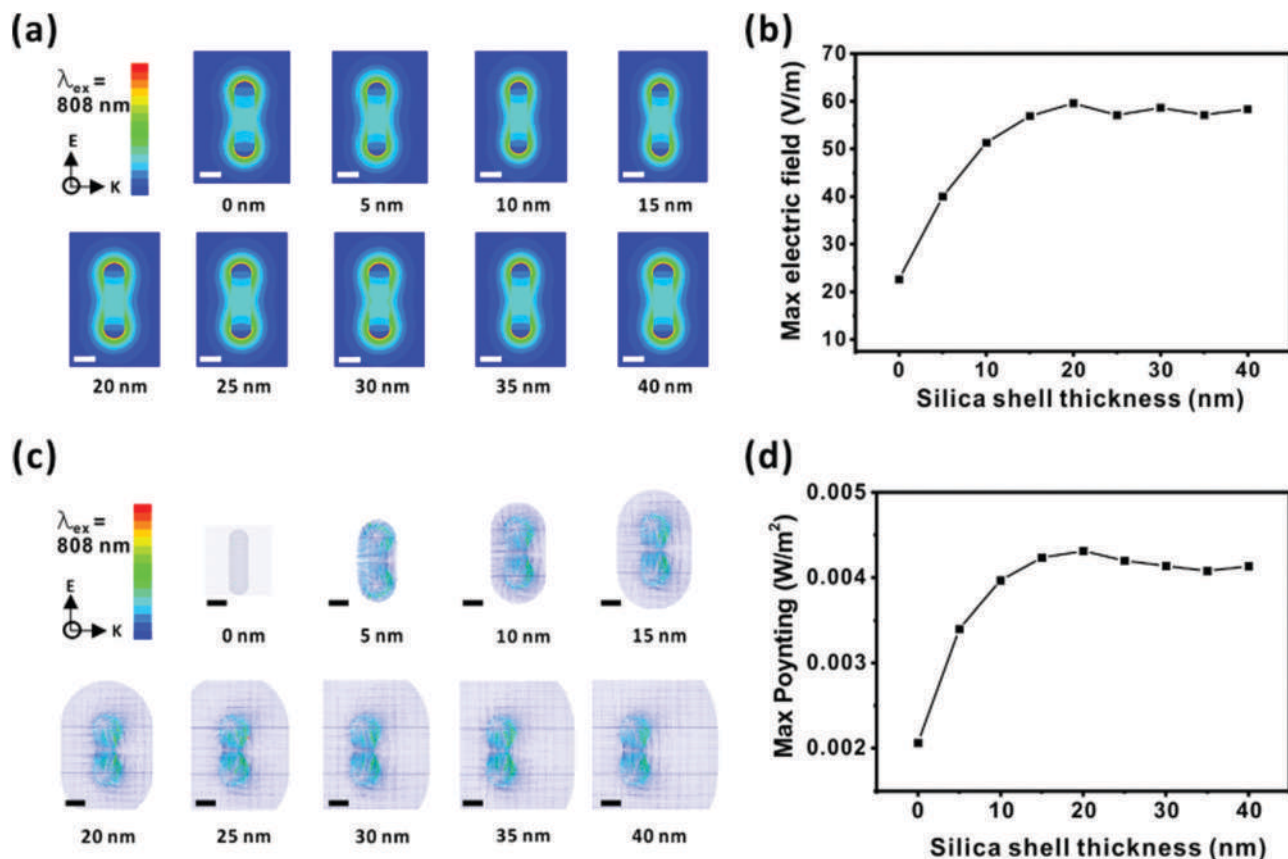
Fig. 5 (a) EM field distributions and (b) a plot of the maximum EM field of CTAB–AuNR and AuNR@SiO$_2$ (5, 10, 15, 20, 25, 30, 35, and 40 nm; scale bars indicate 10 nm); (c) Poynting vector field maps in water; and (d) a plot of the maximum Poynting vector of the AuNRs and AuNR@SiO$_2$ (5, 10, 15, 20, 25, 30, 35, and 40 nm; scale bars indicate 10 nm).

This journal is © The Royal Society of Chemistry 2022

J. Mater. Chem. B, 2022, **10**, 364–372 | **369**

the AuNRs. The EM fields of the AuNRs with a 20 nm-thick silica shell were approximately three times stronger than that of the CRAB–AuNRs, which can produce a localized higher heat gradient between the AuNRs and the media. However, a simple calculation for the EM field on the AuNRs without considering the diffusion property of heat through the interface is not sufficient to accurately reflect the experimental results.

Next, a FEM lab-based simulation was performed by adopting the Poynting vector to calculate the efficiency of thermal radiation depending on the silica shell thickness (Fig. 5(c)).[44] The calculated peak Poynting vector was plotted against an increasing shell thickness (Fig. 5(d)). The peak Poynting vector linearly increased with an increasing shell thickness and reached a peak value at the 20 nm silica shell thickness, and then slightly decreased. The heat diffusion of the AuNRs with a 20 nm-thick silica shell was approximately 2.1 times stronger than that of AuNRs without a silica shell.

Although both calculated results show the highest photothermal efficiency for the 20 nm silica shell thickness, the result of AuNRs with thicker silica shells (>20 nm) is not consistent with that of the experimental results. This is because of the complex nature of the photothermal heat diffusion process through interfaces, in which the conduction process also occurs during the diffusion process.[45] The delayed conduction process in the silica shell (>20 nm) is expected to be more significant in thick silica shell structures. All parameters, such as the EM field distribution, thermal radiation, and conduction, should be simultaneously unified in the calculation to obtain an accurate simulation, which can be a future goal of theoretical research in this field.

3.5 Intracellular uptake efficiency and photothermal-induced cell death

It is important to examine the correlation of improved photothermal efficiency in various situations, such as DW or biological media environments, for future applications. Among the various applications with strong photothermal effects, photoablation with AuNRs and light has been a useful application for cancer therapy.[4,15,18]

To examine the possibility of using an improved photothermal effect for photothermal therapy, the uptake efficiency and the photothermal effect were evaluated with AuNR@SiO$_2$ with silica shell thicknesses of 0–40 nm and HSC-3 cells. First, the uptake efficiency of AuNR@SiO$_2$ depending on the silica thickness was investigated after incubating the same OD of AuNR@SiO$_2$ with HSC-3 cells. Fig. S7 (ESI†) shows that the absorbance of AuNR@SiO$_2$ with SiO$_2$ thicknesses of 20, 25, 30, 35, and 40 nm was approximately 25% lower than that of AuNR@SiO$_2$ with SiO$_2$ thicknesses of 0, 5, 10, and 15 nm because of particle size.[46] To equally uptake AuNR@SiO$_2$ with different silica shell
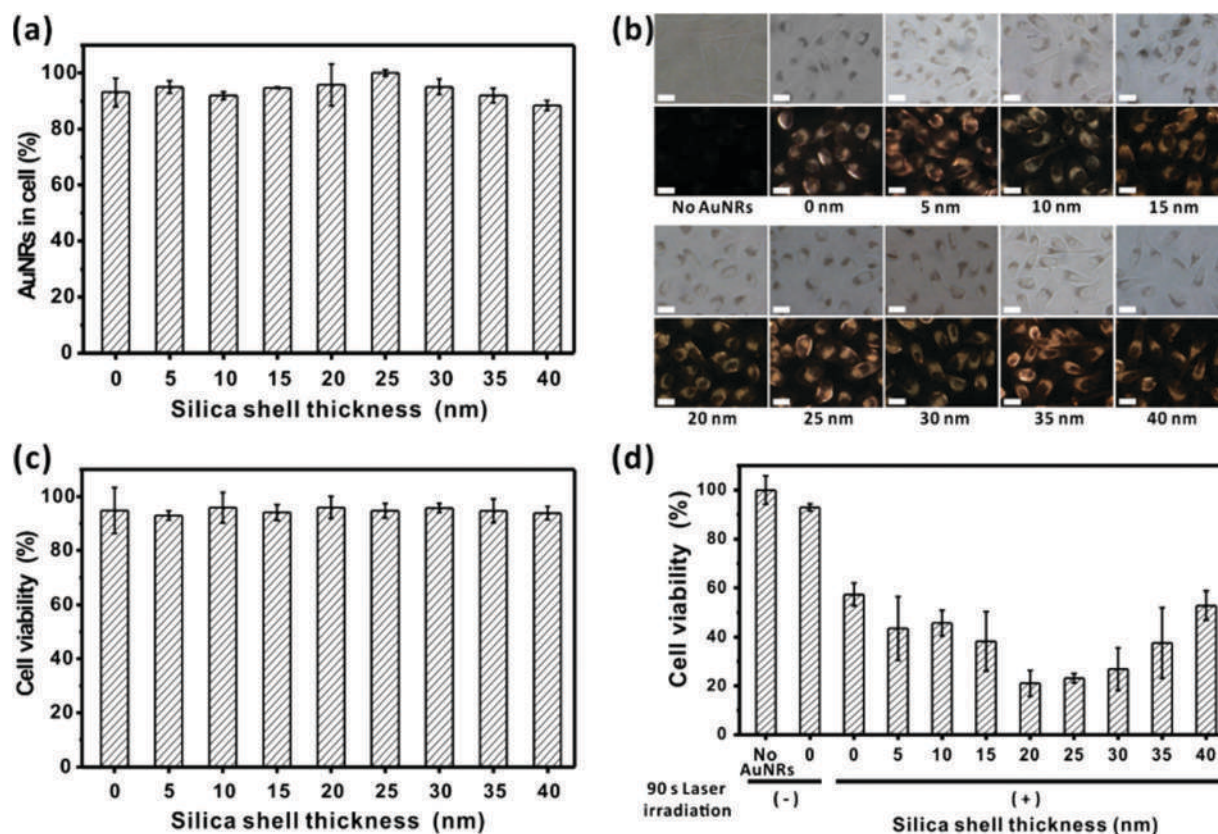

Fig. 6 (a) Amount of CTAB–AuNRs and AuNR@SiO$_2$ (5, 10, 15, 20, 25, 30, 35, and 40 nm) in the HSC-3 cells (measured at 780 nm); (b) bright-field and dark-field images after AuNRs uptake (scale bars indicate 20 μm); (c) cell viability of the CTAB–AuNRs and AuNR@SiO$_2$ (5, 10, 15, 20, 25, 30, 35, and 40 nm); and (d) cell viability of the CTAB–AuNRs and AuNR@SiO$_2$ (5, 10, 15, 20, 25, 30, 35, and 40 nm) after irradiation with a 808 nm CW laser for 90 s.

370 | J. Mater. Chem. B, 2022, 10, 364–372

This journal is © The Royal Society of Chemistry 2022

thickness, the amount of AuNR@SiO$_2$ with thicknesses of 20, 25, 30, 35, and 40 nm (OD 2.0) was varied, then the intracellular absorbance at 780 nm was measured. Fig. 6(a) shows that the amount of CTAB–AuNRs and AuNR@SiO$_2$ with a 5–40 nm silica shell thickness could be controlled at the same level based on the OD values (Fig. 6(a)) or bright-field and dark-field images (Fig. 6(b)). Under these conditions, the cell viability was not significantly different from that of CTAB–AuNRs and AuNR@SiO$_2$ (Fig. 6(c)). The 808 nm laser was illuminated for 90 s on cells containing the same amount of AuNR@SiO$_2$, and cell viability was evaluated. Fig. 6(d) shows that an increased cell death was observed with an increasing silica shell thickness up to 20 nm, but a decreased cell death was observed with an increasing silica shell thickness (>20 nm). The results are highly consistent with the results of the photothermal efficiency performed in DW, indicating that the improved photothermal efficiency of AuNR@SiO$_2$ can be applied to a biological media environment.

4. Conclusions

This study demonstrates a robust synthetic method for AuNR@SiO$_2$ with nanoscale thicknesses ranging from 5–40 nm with selected base and solvent conditions. The photothermal efficiency depends on the silica shell thickness, showing the highest value at a silica shell thickness of 20 nm, which is a 1.45-fold higher photothermal efficiency than that of AuNRs without a silica shell. AuNR@SiO$_2$ showed significantly improved photostability, even after repeated 808 nm laser stimulation. The structure of the AuNRs in AuNR@SiO$_2$ did not change during light illumination and exhibited excellent colloidal stability. In contrast, CTAB–AuNRs were not tolerant to laser illumination, which showed significant changes in the aspect ratio from 4.5 to 3.0, and the disruption of CTAB on the AuNRs was identified by Raman analysis. Furthermore, it was found that the density and morphology of the silica shell were important parameters for obtaining an improved photothermal efficiency and photostability. The low density of the silica shells on the AuNRs showed a low photothermal effect and photostability. The simulation study for the EM field distribution and heat diffusion property showed the highest localized EM field and peak heat diffusion in the 20 nm silica shell thickness. In a cell-based study, AuNR@SiO$_2$ with a 20 nm silica shell thickness showed the most sensitive photothermal effect for cell death. It is expected that the results of this study can provide a clear conclusion regarding the controversy of the silica shell thickness for photothermal efficiency and PA amplitude. The results will be useful for the future design of core/shell based nanomaterials in various field of applications.[47–49]

Conflicts of interest

There are no conflicts of interest to declare.

Acknowledgements

Notes and references

1 M. A. El-Sayed, *Acc. Chem. Res.*, 2001, **34**, 257–264.
2 L. S. Slaughter, W.-S. Chang, P. Swanglap, A. Tcherniak, B. P. Khanal, E. R. Zubarev and S. Link, *J. Phys. Chem. C*, 2010, **114**, 4934–4938.
3 B. N. Khlebtsov, V. A. Khanadeev, A. M. Burov, E. C. Le Ru and N. G. Khlebtsov, *J. Phys. Chem. C*, 2020, **124**, 10647–10658.
4 X. Huang, S. Neretina and M. A. El-Sayed, *Adv. Mater.*, 2009, **21**, 4880–4910.
5 H. Ma, P. M. Bendix and L. B. Oddershede, *Nano Lett.*, 2012, **12**, 3954–3960.
6 H. Chen, L. Shao, Q. Li and J. Wang, *Chem. Soc. Rev.*, 2013, **42**, 2679–2724.
7 Y.-S. Chen, S. J. Yoon, W. Frey, M. Dockery and S. Emelianov, *Nat. Commun.*, 2017, **8**, 15782.
8 W. Yang, J. Noh, H. Park, S. Gwon, B. Singh, C. Song and D. Lee, *Biomaterials*, 2018, **154**, 48–59.
9 Y.-S. Chen, Y. Zhao, S. J. Yoon, S. S. Gambhir and S. Emelianov, *Nat. Nanotechnol.*, 2019, **14**, 465–472.
10 J. H. Son, B. Cho, S. Hong, S. H. Lee, O. Hoxha, A. J. Haack and L. P. Lee, *Light: Sci. Appl.*, 2015, **4**, e280.
11 J. Kim, H. Kim, J. H. Park and S. Jon, *Nanotheranostics*, 2017, **1**, 178–185.
12 G. Baffou and R. Quidant, *Laser Photonics Rev.*, 2013, **7**, 171–187.
13 Y. S. Chen, W. Frey, S. Kim, P. Kruizinga, K. Homan and S. Emelianov, *Nano Lett.*, 2011, **11**, 348–354.
14 Y. S. Chen, W. Frey, S. Kim, K. Homan, P. Kruizinga, K. Sokolov and S. Emelianov, *Opt. Express*, 2010, **18**, 8867–8877.
15 Z. Zhang, L. Wang, J. Wang, X. Jiang, X. Li, Z. Hu, Y. Ji, X. Wu and C. Chen, *Adv. Mater.*, 2012, **24**, 1418–1423.
16 S. Shen, H. Tang, X. Zhang, J. Ren, Z. Pang, D. Wang, H. Gao, Y. Qian, X. Jiang and W. Yang, *Biomaterials*, 2013, **34**, 3150–3158.
17 W. C. Wu and J. B. Tracy, *Chem. Mater.*, 2015, **27**, 2888–2894.
18 C. Li, K. Feng, N. Xie, W. H. Zhao, L. Ye, B. Chen, C. H. Tung and L. Z. Wu, *ACS Appl. Nano Mater.*, 2020, **3**, 5070–5078.
19 S. C. Nguyen, Q. Zhang, K. Manthiram, X. C. Ye, J. P. Lomont, C. B. Harris, H. Weller and A. P. Alivisatos, *ACS Nano*, 2016, **10**, 2144–2151.
20 G. A. Pang, F. Poisson, J. Laufer, C. Haisch and E. Bossy, *J. Phys. Chem. C*, 2020, **124**, 1088–1098.
21 N. D. Burrows, W. Lin, J. G. Hinman, J. M. Dennison, A. M. Vartanian, N. S. Abadeer, E. M. Grzincic, L. M. Jacob, J. Li and C. J. Murphy, *Langmuir*, 2016, **32**, 9905–9921.
22 B. Nikoobakht and M. A. El-Sayed, *Chem. Mater.*, 2003, **15**, 1957–1962.
23 H. Moon, D. Kumar, H. Kim, C. Sim, J. H. Chang, J. M. Kim, H. Kim and D. K. Lim, *ACS Nano*, 2015, **9**, 2711–2719.
24 D. K. Roper, W. Ahn and M. Hoepfner, *J. Phys. Chem. C*, 2007, **111**, 3636–3641.
25 Q. Tian, F. Jiang, R. Zou, Q. Liu, Z. Chen, M. Zhu, S. Yang, J. Wang, J. Wang and J. Hu, *ACS Nano*, 2011, **5**, 9761–9771.
26 Y. Liu, D. Zhu, Y. Hu, M. T. Swihart and W. Wei, *Langmuir*, 2018, **34**, 13905–13909.

This journal is © The Royal Society of Chemistry 2022

J. Mater. Chem. B, 2022, **10**, 364–372 | 371

27 P. B. Johnson and R. W. Christy, *Phys. Rev. B: Solid State*, 1972, **6**, 4370–4379.

28 V. Pellas, D. Hu, Y. Mazouzi, Y. Mimoun, J. Blanchard, C. Guibert, M. Salmain and S. Boujday, *Biosensors*, 2020, **10**, 146.

29 N. S. Abadeer, M. R. Brennan, W. L. Wilson and C. J. Murphy, *ACS Nano*, 2014, **8**, 8392–8406.

30 E. Mine, A. Yamada, Y. Kobayashi, M. Konno and L. Liz-Marzán, *J. Colloid Interface Sci.*, 2003, **264**(2), 385–390.

31 O. Niitsoo and A. Couzis, *J. Colloid Interface Sci.*, 2011, **354**(2), 887–890.

32 I. Pastoriza-Santos, J. Perez-Juste and L. M. Liz-Marzan, *Chem. Mater.*, 2006, **18**, 2465–2467.

33 L. M. Liz-Marzan, M. Giersig and P. Mulvaney, *Langmuir*, 1996, **12**, 4329–4335.

34 M. Hu, X. Wang, G. V. Hartland, V. Salgueirino-Maceira and L. M. Liz-Marzan, *Chem. Phys. Lett.*, 2003, **372**, 767–772.

35 M. Nikbakht, *J. Quant. Spectrosc. Radiat. Transfer*, 2018, **221**, 164–171.

36 H. Gokce and S. Bahceli, *Opt. Spectrosc.*, 2013, **115**, 632–644.

37 P. Bock and N. Gierlinger, *J. Raman Spectrosc.*, 2019, **50**, 778–792.

38 C. Mahoney, K. Park, A. Jawaid, B. Kowalski, A. Gillman, V. Tondiglia, B. Treml, T. White and R. A. Vaia, *J. Mater. Chem. C*, 2018, **6**, 7157–7169.

39 M. Gordel, J. Olesiak-Banska, K. Matczyszyn, C. Nogues, M. Buckle and M. Samoc, *Phys. Chem. Chem. Phys.*, 2014, **16**, 71–78.

40 C. Hanske, M. N. Sanz-Ortiz and L. M. Liz-Marzán, *Adv. Mater.*, 2018, **30**, 1707003.

41 L. Xie, B. Dong, Z. Jiang, Y. Wang, T. Liu and X. Bai, *J. Mater. Res.*, 2011, **26**, 2414–2419.

42 T. Gan, J. Li, L. Xu, S. Guo, A. Zhao and J. Sun, *Microchim. Acta*, 2020, **187**, 291.

43 L. Ernawati, T. Ogi, R. Balgis, K. Okuyama, M. Stucki, S. C. Hess and W. J. Stark, *Langmuir*, 2016, **32**, 338–345.

44 S. J. Blundell and K. M. Blundell, *Concepts in Thermal Physics*, Oxford University Press, 2006.

45 W. Dai, Y. Gan and D. Hanaor, *Appl. Mech. Mater.*, 2016, **846**, 500–505.

46 L. Tang, N. P. Gabrielson, F. M. Uckun, T. M. Fan and J. J. Cheng, *Mol. Pharmaceutics*, 2013, **10**, 883–892.

47 W. Liu, Z. Zhu, K. Deng, Z. Li, Y. Zhou, H. Qiu, Y. Gao, S. Che and Z. Tang, *J. Am. Chem. Soc.*, 2013, **135** 9659–9664.

48 D. Zheng, X. Pang, M. Wang, Y. He, C. Lin and Z. Lin, *Chem. Mater.*, 2015, **27**, 5271–5278.

49 M. Wang, X. Pang, D. Zheng, Y. He, L. Sun, C. Lin and Z. Lin, *J. Mater. Chem. A*, 2016, **4**, 7190–7199.

372 | *J. Mater. Chem. B*, 2022, **10**, 364–372

This journal is © The Royal Society of Chemistry 2022